

RESEARCH LETTER

10.1002/2014GL061005

Key Points:

- Waves are a major contributor to extreme sea levels at island shorelines
- Fringing reefs exert a strong control on extreme wave-driven water levels
- Extreme water levels at atolls will increase significantly with sea level rise

Correspondence to:

M. A. Merrifield,
markm@soest.hawaii.edu

Citation:

Merrifield, M. A., J. M. Becker, M. Ford, and Y. Yao (2014), Observations and estimates of wave-driven water level extremes at the Marshall Islands, *Geophys. Res. Lett.*, 41, 7245–7253, doi:10.1002/2014GL061005.

Received 26 JUN 2014

Accepted 25 SEP 2014

Accepted article online 28 SEP 2014

Published online 20 OCT 2014

Observations and estimates of wave-driven water level extremes at the Marshall Islands

M. A. Merrifield¹, J. M. Becker², M. Ford³, and Y. Yao⁴

¹Department of Oceanography, University of Hawaii at Manoa, Honolulu, Hawaii, ²Department of Geology and Geophysics, University of Hawaii at Manoa, Honolulu, Hawaii, ³School of Environment, University of Auckland, Auckland, New Zealand, ⁴School of Hydraulic Engineering, Changsha University of Science and Technology, Changsha, China

Abstract Wave-driven extreme water levels are examined for coastlines protected by fringing reefs using field observations obtained in the Republic of the Marshall Islands. The 2% exceedence water level near the shoreline due to waves is estimated empirically for the study sites from breaking wave height at the outer reef and by combining separate contributions from setup, sea and swell, and infragravity waves, which are estimated based on breaking wave height and water level over the reef flat. Although each component exhibits a tidal dependence, they sum to yield a 2% exceedence level that does not. A hindcast based on the breaking wave height parameterization is used to assess factors leading to flooding at Roi-Namur caused by an energetic swell event during December 2008. Extreme water levels similar to December 2008 are projected to increase significantly with rising sea level as more wave and tide events combine to exceed inundation threshold levels.

1. Introduction

Low-lying atoll islands are especially vulnerable to sea level rise combined with extreme water level events due to swell and storm surges. The impacts were clearly evident during December 2008, when severe coastal flooding occurred at island and atoll nations in the western tropical Pacific and in particular at the Republic of the Marshall Islands (RMI). The flooding resulted from high-amplitude swell waves generated by strong winds to the northeast of the region [Hoeke *et al.*, 2013]. Extreme water levels were reached as high waves combined with high tides, leading to coastal breaching on north and east facing shorelines. Many of the impacted areas, such as the atoll islands of RMI, are protected by fringing reefs, which are shallow (exposed at low tide), wide (hundreds of meters), carbonate platforms with steep ocean-facing reef faces. Fringing reefs provide natural shoreline protection against wave events, with the majority of incident swell energy dissipated at the outer reef [Ferrario *et al.*, 2014]. Assessments and projections of wave-driven inundation at atoll islands require an understanding of wave transformation in all energetic frequency bands over fringing reef platforms for different still water levels over the reef.

Munk and Sargent [1948] gave an early description of the impact of waves at atoll coastlines, noting the super elevation of water levels shoreward of the surf zone. This wave setup effect and its relationship to breaking incident waves have been studied extensively for reef-fringed shorelines, leading to analytic solutions relating incident wind wave heights to setup levels [Tait, 1972; Gourlay, 1996a; Vetter *et al.*, 2010; Monismith *et al.*, 2013; Becker *et al.*, 2014a]. The contribution of high-frequency sea and swell (SS) waves and low-frequency infragravity (IG) waves on runup at reef shorelines was studied by Gourlay [1996a], who noted that the variable swash component of runup was a major contributor to coastal flooding events. Depth-limited breaking determines SS wave heights over shallow reef flats, with additional frictional decay occurring across the reef flat [Péquignet *et al.*, 2011]. Observed IG and SS wave heights are comparable over fringing reefs [Péquignet *et al.*, 2011; Pomeroy *et al.*, 2012], and IG cross-reef standing and partially standing modes have been observed at various locations [Nakaza and Hino, 1991; Lugo-Fernandez *et al.*, 1998; Péquignet *et al.*, 2009; Ford *et al.*, 2013].

Hoeke *et al.* [2013] used a regional wave model to simulate the impact of high swell on Pacific Islands during the December 2008 flooding event. The wave influence on coastal extreme water levels was estimated by shoaling model wave heights to breaking depth using energy flux conservation and scaling the breaking wave height by 20% to estimate coastal setup. SS and IG waves were not considered. Storlazzi *et al.* [2011] demonstrated how wave setup and SS wave heights increase as water level increases over a fringing reef

based on numerical model simulations, but the influence of IG waves was not considered in that study. *Torres-Freyermuth et al.* [2012] found that infragravity energy contributed significantly to extreme water levels for the Puerto Morelos fringing reef lagoon based on numerical simulations.

An empirical parameterization of extreme wave runup on natural beaches was given by *Stockdon et al.* [2006] using video data sets from 10 beaches on continental shorelines. Extreme runup, defined by *Stockdon et al.* [2006] as the 2% exceedence water level at the shoreline above the still water level, was estimated as a function of wave setup and variable swash at SS and IG frequencies. Parameterizations of setup and swash were made based on incident deep water wave height and wavelength and beach slope. Applications of the 2% exceedence runup for beaches fronted by a fringing reef have not been tested; however, it has been established that water level over fringing reefs similar to those present at RMI plays an important control on shoreline setup [*Becker et al.*, 2014a], SS wave heights [*Péquignot et al.*, 2011], and IG wave heights [*Péquignot et al.*, 2009]. The influence of water level on setup and swash are not included in the *Stockdon et al.* [2006] parameterizations, which were developed for sand beaches without reef structures.

In this study, we apply the methodology of *Stockdon et al.* [2006] to develop a parameterization for extreme wave-driven water levels at atoll shorelines protected by fringing reefs. We are concerned with the outer atoll shoreline, as opposed to the lagoon shoreline, which generally are protected from energetic waves. Field observations of waves and water level at Roi-Namur island at the Kwajalein Atoll and on the atoll island of Majuro during 2010–2011 are used to develop empirical relationships relating incident SS wave heights and water level over the reef to the 2% exceedence water level near the shoreline. Unlike *Stockdon et al.* [2006], we do not consider extreme wave runup over a sloping beach; instead, we focus on measurements of 2% exceedence water level at a location on the reef flat near the shoreline. Visual inspections suggest that these observations are representative of conditions at the shore. The irregularity of natural and man-made shoreline structures at the study sites makes it difficult to characterize a representative runup. The results from the field study are used to assess the factors contributing to the December 2008 flooding event and others like it, as well as the risk of wave-driven coastal flooding at RMI for higher sea levels.

2. Field Observations

Field experiments were conducted during November 2010 to May 2011 at Majuro atoll (Figure 1a) in the western tropical Pacific. A cross-shore sensor array was deployed on the fringing reef adjacent to the College of the Marshall Islands (CMI) on the east side of the atoll (Figures 1b and 1c). The CMI reef flat is ~250 m wide, ~0.8 m deep, with a shoreline armored with revetment and large block seawalls. The second experiment site was at Roi-Namur island at the northern tip of the Kwajalein Atoll (Figure 1d), approximately 400 km northwest of Majuro. The cross-shore sensor array (Figures 1e and 1f) was deployed on the ~350 m wide, ~0.8 m deep, fringing reef flat. The tides at CMI and Roi are mixed semidiurnal and diurnal with a mean range of 1 m and a typical spring range of 1.6 m. The reef flats at both sites were completely submerged at the mean higher high water level computed over the course of the experiment and exposed during mean lower low water (Figures 1c and 1f). The experiment took place with mean sea level at Kwajalein ~0.07 m above the 1983–2001 epoch. A more detailed description of the experiment sites is given in *Becker et al.* [2014a].

In this study we consider only the Seabird 26plus wave and water level recorders with Paroscientific Digi-quartz pressure measurements from sensors 2 and 7 at Majuro, denoted as MC2 and MC7 (Majuro, C deployment, sensor number), and sensors 1 and 5 at Roi (RC/c1 and RC/c5, where the deployment was split into two parts, C and c, due to a displacement of sensor 5 during a wave event on 20 January 2011). A description of all sensors used in the experiment (Figures 1c and 1f) is given in *Becker et al.* [2014a]. MC7 and RC/c5 are used to provide significant wave heights on the reef face, denoted as H_f (Figures 2a and 2f). Sensors MC2 and RC/c1 are used to define the wave (Figures 2d, 2e, 2i, and 2j) and water level (Figures 2b, 2c, 2g, and 2h) variability near the shoreline. All data were collected at 1 Hz sample frequency over 1.5 h burst samples every 3 h. Burst samples are not included in the analysis when water level over a sensor is less than 0.1 m. An inverse barometer correction is made using atmospheric pressure measurements provided by the NOAA Center for Operational Products and Services (CO-OPS) for Kwajalein and the National Tidal Centre, Australia, for Majuro.

SS surface elevations are estimated from detided bottom pressure measurements using linear wave theory. Setup ($\bar{\eta}$) at MC2 and RC/c1 is computed following *Becker et al.* [2014a]. Significant wave heights are

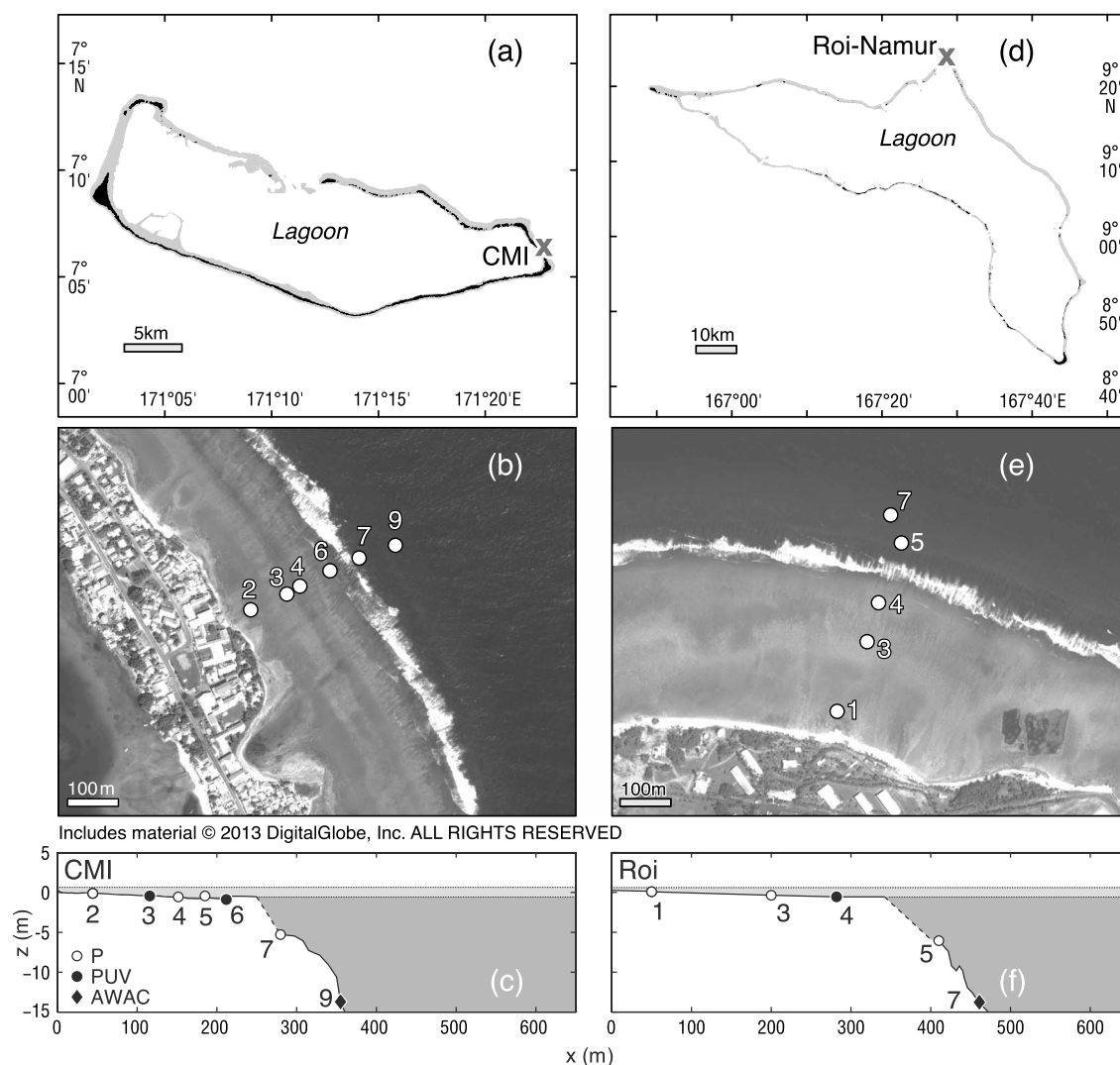


Figure 1. (a) Map of the experiment site at the College of the Marshall Islands (CMI), Majuro atoll, (b) a satellite image showing the CMI sensor array, (c) the sensor type and cross-shore position at CMI. The band of water levels at the surface represents mean lower low water (bottom of light band) and mean higher high water during the experiment. The dashed line in the bathymetry profile is linearly interpolated between the shallowest depth sounding and the estimated edge of the reef flat from satellite images. (d–f) The same for Roi-Namur, Kwajalein Atoll, RMI.

computed over 15 min intervals as 4 times the standard deviation from the surface elevation spectrum integrated between 0.033 to 0.35 Hz for SS waves (referred to as H_{ss} for the nearshore sensors at MC2 and RC/c1) and 0.0011 to 0.033 Hz for IG waves (H_{ig} at MC2 and RC/c1). The minimum spectral energy between IG and SS peaks is approximately at 0.033 Hz. The SS significant wave height at the reef face (Figures 2a and 2f) ranged from 1 to 2.5 m, with slightly higher values at Roi. Peak wave periods were between 6 to 24 s at CMI and 4 to 21 s at Roi with arrivals primarily from the northeast.

Extreme water levels near the shoreline caused by waves (η_2 , Figures 2b and 2g) are estimated as the 2% exceedence level of 1 Hz sampled surface elevation over 15 min records, with mean sea level, the tides, and nonwave-related sea level anomalies removed. Our estimate based on the continuous record differs from Stockdon *et al.* [2006], who considered 2% exceedence of runup maxima. An estimate based on water level maxima would increase η_2 by 5–8% over the values reported in this study. Following Stockdon *et al.* [2006], we confirm that η_2 is related to wave setup ($\bar{\eta}$) and the standard deviation of surface elevation over the SS and IG frequency bands by

$$\hat{\eta}_2 = \bar{\eta} + b\sigma, \quad (1)$$

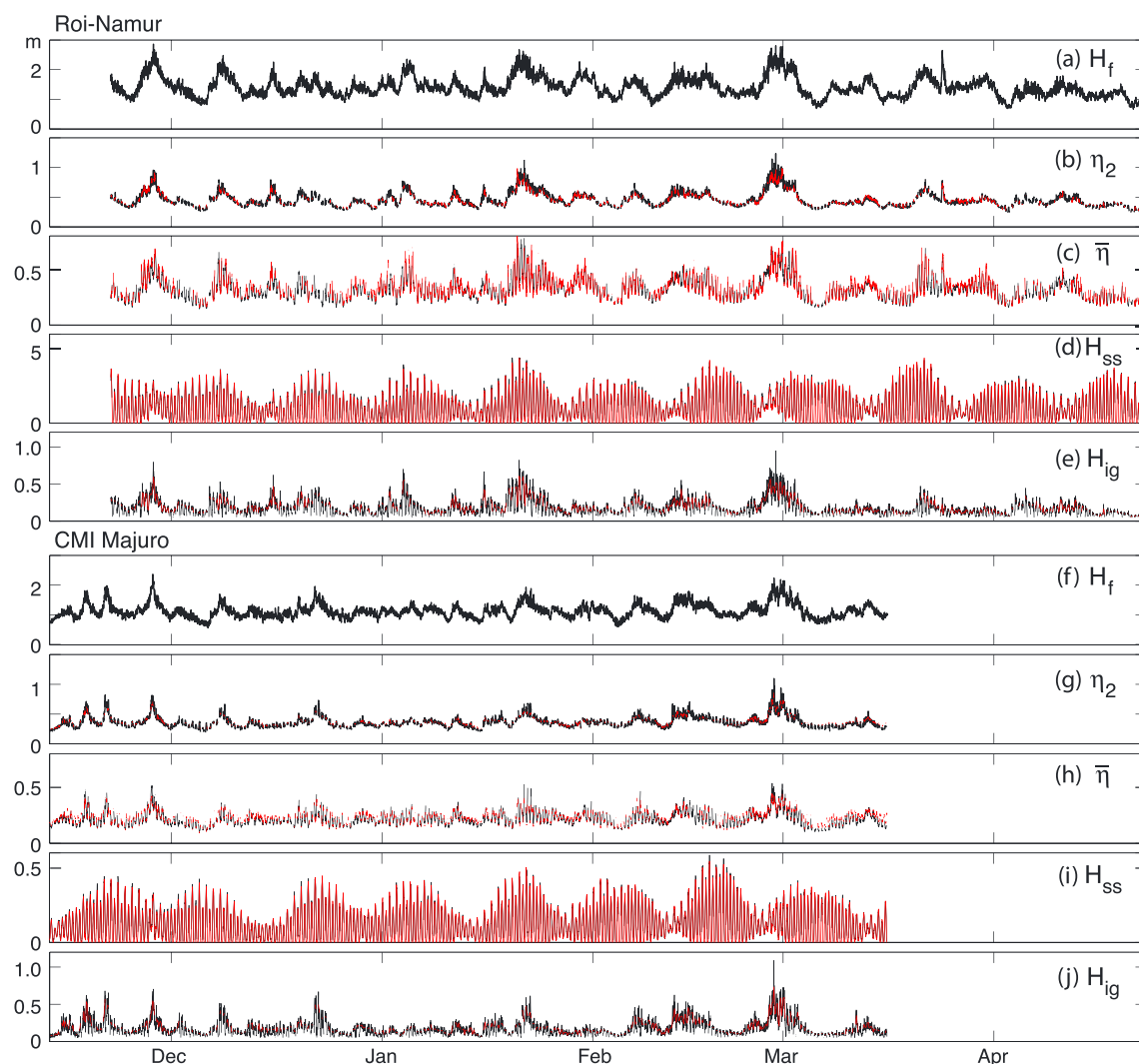


Figure 2. Measurements of waves and water level at Roi-Namur during 2010–2011 including (a) sea-swell significant wave height (H_f) at 6 m depth (sensor 5, Figure 1f), (b) observed (black, η_2) and estimated (red, (1)) 2% exceedence water level, (c) observed ($\bar{\eta}$) and estimated (3) setup, (d) observed (H_{ss}) and estimated (\hat{H}_{ss}) sea-swell significant wave height, and (e) observed (H_{ig}) and estimated (from (6)) infragravity significant wave height, with Figures 2b–2e all from sensor 1 (Figure 1c). (f–j) The same measurements at CMI Majuro, with H_f (Figure 2f) from sensor 7 (Figure 1c) and (Figures 2g–2j) from sensor 2.

where $\sigma = 0.25 \sqrt{H_{ss}^2 + H_{ig}^2}$. A least squares fit of $\eta_2 - \bar{\eta}$ on σ , for CMI and Roi combined, yields $b = 2.22$ with $r^2 = 0.99$. Stockdon *et al.* [2006] found that the swash observations in their study exhibited a positive skewness, which causes a departure from a normal distribution. The same applies to nearshore water level variations over the CMI and Roi fringing reefs, which have an average skewness of 0.36 at MC2 and RC/c1, leading to $b > 2.05$, the 2% exceedence value expected for a normally distributed random variable.

3. Parameterizations of Extreme Water Level

We consider two parameterizations for the extreme water level η_2 . The first, $\tilde{\eta}_2$, is estimated from the breaking wave height on the reef face, \hat{H}_b , which is obtained from H_f assuming conservation of energy flux for the nonnormally incident waves present at each site and the breaking condition described in Becker *et al.* [2014a]. A linear dependence is used:

$$\tilde{\eta}_2 = b_1 \hat{H}_b + b_0, \quad (2)$$

with a least squares fit yielding $b_1, b_0 = 0.31 \pm 0.05, -0.10 \pm 0.09$ for Roi and $0.33 \pm 0.07, -0.14 \pm 0.10$ for CMI, with 95% confidence intervals included assuming an independent data point every 2.5 days. The \hat{H}_b

based parameterization $\tilde{\eta}_2$ is significantly (99%) correlated with the observed η_2 , with $r^2 = 0.84$ for Roi and CMI combined. Thus, as a general rule, the extreme water level is approximately 32% of the breaking wave height at each site, reduced by approximately 0.12 m.

The second estimate for the extreme water level is based on (1), with separate parameterizations for nearshore setup and significant wave heights in the SS and IG frequency bands. Setup is estimated from the breaking wave height following *Becker et al.* [2014a] as

$$\hat{\eta} = \frac{5}{32} \gamma_s (\hat{H}_b - 1.2H_{ss}), \quad (3)$$

where γ_s is the ratio of breaking significant wave height to breaking water depth, which differs from the γ_b in *Becker et al.* [2014a] (who used RMS wave heights) by a factor of $\sqrt{2}$. The mean γ_s during the deployment is 1.3 at Roi and 1.1 at CMI. As discussed in *Becker et al.* [2014a], γ_s varies with the tide with higher γ_s 's at low tide compared to high tide. A marked tidal dependence is evident in the observed and estimated setup at both sites, due to the tidal dependence of both H_{ss} and γ_s , with higher setup at low tide for a given breaking wave height and lower setup at high tide [*Becker et al.*, 2014a]. The observed and estimated setups are significantly correlated, with $r^2 = 0.94$ for Roi and CMI combined.

SS band waves on the reef are strongly depth limited, as they are on other fringing reef flats [*Péquignot et al.*, 2011], with H_{ss} varying with total water level over the reef due to the tide and wave setup (Figures 2d and 2i). For general reef applications, a parameterization similar to *Péquignot et al.* [2011] that accounts for depth-limited breaking and frictional decay over the reef flat is recommended. For our purposes, we employ a direct empirical relationship relating observed H_{ss} and reef flat water level, h_r . A second-order fit is significantly better than a linear fit; hence, we use $\hat{H}_{ss} = c_2 h_r^2 + c_1 h_r + c_0$. A least squares fit for the Roi and CMI observations combined yields $(c_2, c_1, c_0) = (0.10 \pm 0.04, 0.26 \pm 0.04, 0.00 \pm 0.01)$. The observed and estimated significant wave heights are significantly correlated, with $r^2 = 0.99$ (Figures 2d and 2i). We note that the estimate \hat{H}_{ss} depends on water level, including setup, and the estimate of setup depends on H_{ss} ; hence, an iterative solution is required as discussed in *Becker et al.* [2014a].

For the steep reef faces of CMI and Roi, the observed IG energy on the reef flat may be modeled as dynamic setup [*Becker et al.*, 2014b]. While bound waves incident from offshore also may impact IG motions on fringing reef flats, the peak response at the shoreline is consistent with breakpoint forcing [*Péquignot et al.*, 2014]. For a parameterization of H_{ig} , the point break dynamics of *Becker et al.* [2014a] are extended to the linear long-wave equations for an idealized step reef of length L and projected onto the spatial normal modes yielding a forced, damped oscillator equation for the time-dependent modal amplitudes, $\eta_n^{ig}(t)$,

$$\frac{d^2 \eta_n^{ig}}{dt^2} + D \frac{d \eta_n^{ig}}{dt} + \omega_n^2 \eta_n^{ig} = (-1)^n \frac{3}{32} g \gamma_s k_n h_r \hat{H}_b(t). \quad (4)$$

In (4), $k_n = (2n + 1)\pi/2L$ is the modal wave number for mode n , $\omega_n = \sqrt{gh_r} k_n$ is the modal frequency, D is a damping coefficient, g is gravity, and $\hat{H}_b(t)$ is the time-dependent breaking wave height obtained from the envelope (Hilbert transform) of the shoaled reef face wave height. The IG-free surface elevation time series are obtained from the inverse Fourier cosine transform

$$\eta^{ig}(x, t) = \frac{2}{L} \sum_{n=0}^{\infty} \eta_n^{ig}(t) \cos(k_n x). \quad (5)$$

Solving (4) using a Fourier transform in time (i.e., $\mathcal{F}[\hat{H}_b(t)] = \hat{H}_b(\omega)$) and inverting both transforms, we find

$$\eta^{ig}(x, t) = \sum_{n=0}^{\infty} \mathcal{F}^{-1} \left[B_n(\omega) \hat{H}_b(\omega) \right] \cos(k_n x), \quad (6)$$

$$B_n(\omega) = \frac{(-1)^n 3g \gamma_s k_n h_r / 8L}{\omega^2 - \omega_n^2 - iD\omega}, \quad (7)$$

where \mathcal{F}^{-1} is the inverse Fourier transform in time. Equation (6) yields a one parameter (D) model of the IG free surface elevation on the reef flat. The estimated IG band significant wave height, \hat{H}_{ig} , at MC2 and RC/c1 is 4 times the standard deviation of $\eta^{ig}(x, t)$ in the IG frequency range, with $x = 50$ m and 44 m at Roi and CMI, respectively. We use the first two normal modes ($n = 0, 1$) in (6) with $D = 0.005$ at Roi and

$D = 0.007$ at CMI. The estimated and observed IG significant wave heights are significantly correlated at both CMI and Roi, with $r^2 = 0.78$ (Figures 2e and 2j).

Combining the estimates of $\hat{\eta}$, \hat{H}_{ss} , and \hat{H}_{ig} , we obtain from (1) an estimate of the extreme water level, $\hat{\eta}_2$, that is in better agreement with the observations (r^2 is 0.93) than $\tilde{\eta}_2$ obtained directly from \hat{H}_b ($r^2 = 0.84$). The observed and estimated extreme wave-driven water levels do not show a strong tidal dependence (Figure 2), implying that the 2% exceedence level is not impacted by water level changes across the tidal range. In contrast, the components of extreme water level do show a marked tidal dependence, particularly setup, $\bar{\eta}$, and H_{ss} . As the tidal level increases, H_{ss} on the reef flat increases which in turn causes setup to decrease (3). Setup also is lower during high tide than low tide for a fixed H_f because of the tidal dependence of γ_s [Becker *et al.*, 2014a]. H_{ig} varies less with the tide than the other two components, but it does so through a dependence on $\gamma_s h_f$ (equation (7)). The tidal influence amongst the components cancel, however, when summed together to form η_2 . Thus, high tides or background still water levels will have a larger net contribution to η_2 from time-varying wave components and smaller from the mean water level change due to setup, with the opposite occurring during low water level. We emphasize that the higher wave energy on the reef flat during high tide may lead to stronger swash variability at the shoreline than would be the case at low tide, which is not accounted for in the present analysis. Specifically, even though η_2 does not exhibit a water level dependence, that may not necessarily be the case for coastal runoff.

4. Hindcasts and Projections of Extreme Water Level

The parameterization of extreme water level based on breaking wave height is used to assess the December 2008 flooding event at Roi. We use $\tilde{\eta}_2$ obtained from breaking wave height (2) instead of the estimate based on (1) because we do not have direct information on the spectral behavior of \hat{H}_b needed in (6). WaveWatch III model hindcasts [Durrant *et al.*, 2013] are used to estimate deep water significant wave height, H_o , dominant wave period, T_o , and dominant wave direction, θ_o , at a model grid point just north of Roi-Namur. The deep water wave heights are shoaled to breaking depth to obtain \tilde{H}_b at the Roi study site as

$$\tilde{H}_b = [H_o^2 T_o (4\pi)^{-1} \cos(\theta_o - \theta_N) \sqrt{\gamma_s g}]^{2/5}, \quad (8)$$

where $\theta_N = 20^\circ$, the shore-normal angle at Roi. Wave conditions for which $\cos(\theta_o - \theta_N) < 0$ are not included. The hourly time series from the NOAA tide gauge in Kwajalein Atoll is used to specify tidal and sea level variations, which we find to be representative of water level variations measured seaward of the breaker zone at RC/c7. In addition, sea level in the Kwajalein Atoll lagoon does not show an obvious relationship to H_o , suggesting that the record reflects still water level changes. The lack of a setup signal in atoll tide gauges in the region during the December 2008 event was noted by Hoeke *et al.* [2013]. Based on approximate land elevation estimates made during the 2010–2011 field study at Roi-Namur, we estimate that inundation impacts are likely to occur when water levels exceed 2 m above mean sea level.

The estimated $\tilde{\eta}_2$, (2), is added to the observed still water level record from the tide gauge to yield a time series of total extreme water levels associated with waves, tides, and nonwave sea level anomalies for the month of December 2008 (Figure 3a). The estimated breaking wave height during the event peaked at 5.1 m at 07:00 8 December (UTC), with heights in excess of 4.5 m for a 24 h period beginning on 7 December. The wave event occurred just after neap tide, so the tidal range was roughly half that during the following spring tide. The combination of the tides, sea level anomaly, and $\tilde{\eta}_2$ resulted in total extreme water levels of 1.9 m for high tides on 8 and 9 December during the wave event. Based on the uncertainties of the empirical parameters used to estimate $\tilde{\eta}_2$ and an \tilde{H}_b model uncertainty of 0.2 m obtained by estimating the standard deviation of the model minus observed wave heights during the Roi field experiment, the standard deviation for $\tilde{\eta}_2$ is ~ 0.1 m for the peak water levels. Hence, the estimated extreme water levels are within approximately one standard deviation error of the specified inundation level when flooding was observed to have occurred. The combination of high tides and wave-driven extreme water level $\tilde{\eta}_2$ were required to approach the estimated inundation level, as $\tilde{\eta}_2$ contributed 1.5 m and 1.3 m of water level during the two peak high tides, which measured 0.4 m and 0.6 m. A second wave event during 12–13 December resulted in extreme water levels similar to 8 December. The weaker wave heights during the second event were compensated by higher tide levels near spring tide conditions. Popular media reports confirm the occurrence of flooding at RMI during both wave events (http://www.spc.int/ppapd/index.php?option=com_content&task=view&id=318&Itemid=2, <http://pidp.org/archive/2008/December/12-17-01.htm>).

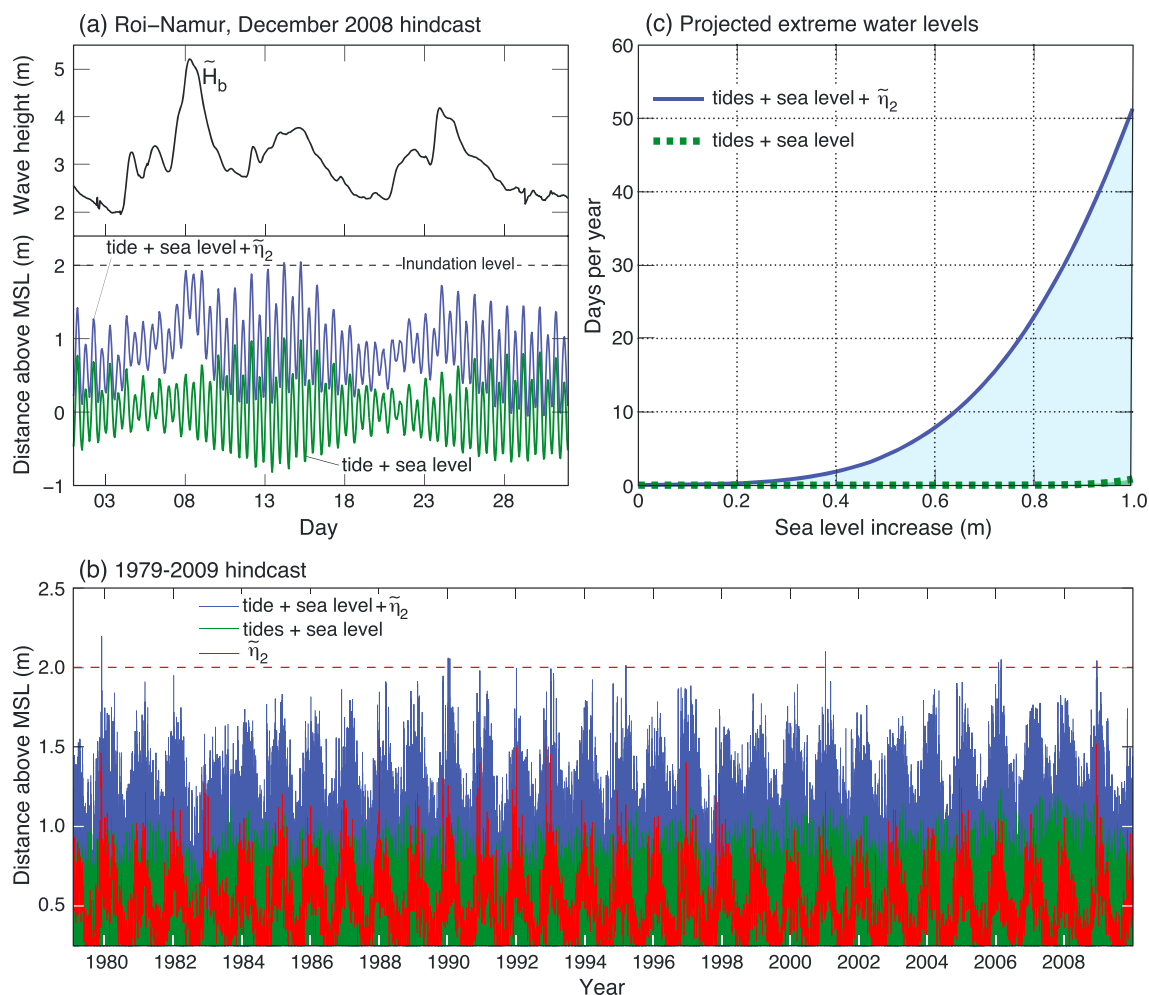


Figure 3. (a) Reconstruction of the December 2008 flooding event at Roi-Namur based on tide + sea level from the Kwajalein tide gauge, breaking wave height (\tilde{H}_b) estimated by shoaling deep water wave heights from the WaveWatch III hindcast (8), and estimated 2% exceedance water level ($\tilde{\eta}_2$) based on (2). Inundation is estimated to occur when tide + sea level + $\tilde{\eta}_2 \geq 2$ m above mean sea level. (b) Same as Figure 3a for the time period February 1979 through December 2009. (c) The cumulative number of days per year that tides + sea level and tides + sea level + $\tilde{\eta}_2$ are ≥ 2 m at Roi-Namur for sea level increases between 0 and 1 m. The estimate is based on adding constant water level increments to the time series depicted in Figure 3b.

The hindcast of $\tilde{\eta}_2$ next is evaluated over the period February 1979 through December 2009 (Figure 3b). As was the case during December 2008, all predicted inundation events occur during energetic winter wave events over the 31 year time period. Tidal elevation and sea level alone never exceed 1.3 m, well below the inundation threshold. The importance of the co-occurrence of high tide and high waves is again evident, as some relatively modest wave events led to high extreme water levels because they occurred near peak spring tide (e.g., January 2001), whereas some particularly energetic wave events did not reach threshold because they occurred at low tide (e.g., December 1996). The largest predicted extreme water level, 2.2 m, occurred on 3 December 1979 [Ginoza, 1979]. The estimated $\tilde{\eta}_2$ level (1.3 m) during the peak of the event was similar to the December 2008 flooding events; however, the still water level was higher (0.9 m). Even though regional sea level has been rising at a high rate since the early 1990s [Merrifield et al., 2012], the number of estimated inundation events has not increased accordingly, highlighting the importance of wave events over still water levels in determining extremes over this time period. The standard deviation of hourly still water level anomalies at Kwajalein is < 0.1 m. The wave model results suggest that extreme wave events were prevalent during the late 1980s and early 1990s and less frequent subsequently.

The amount of wave-induced flooding at Roi as a function of increased mean sea level is considered based on the WaveWatch III model results. We compute $\tilde{\eta}_2$ from (2) using breaking wave height estimated from

the wave model hindcasts (8) and the Kwajalein tide gauge time series from 1979 through 2009. Over the 31 year record, the average time per year, measured in cumulative days, for which the total extreme water level exceeds 2 m is compiled. We then repeat the calculation for different mean sea level increases in the 0 to 1 m range. The result emphasizes the importance of the wave contribution to coastal flooding as sea level rises, with the average number of flooding days increasing nearly exponentially when $\tilde{\eta}_2$ is included (Figure 3b). For comparison, the same estimate is made without $\tilde{\eta}_2$, in which case a 0.9 m increase in sea level is required to cause a significant increase in the number of flooding days each year due to tides, sea level anomalies, and sea level rise. In contrast, a significant increase in flooding days is apparent after only a 0.3 m rise in sea level when $\tilde{\eta}_2$ is included, reaching 50 cumulative days of flooding each year for a 1.0 m rise in sea level. We note that changes in wave climatology for future climate states may further augment these results.

5. Discussion

The parameterization of 2% exceedence level based on breaking wave height (equation (2)) is useful for assessing extreme conditions at the two RMI sites and presumably at other sites with similar reef dimensions and roughness characteristics. An advantage of $\tilde{\eta}_2$ over the component estimate $\hat{\eta}_2$ (equation (1)) is that the breaking wave height envelope spectrum in (6) is not required, which is not routinely available from spectral wave models; $\tilde{\eta}_2$ also has the advantage of being independent of the water level over the reef flat, which may be difficult to assess in regions lacking a tide gauge. The extreme wave-driven water levels obtained here scale as $\sim 32\%$ of the breaking wave height, with a ~ -0.12 m offset adjustment. These levels are on average 48% higher than the wave-driven setup contribution, i.e., the SS and IG wave components add a 48% increase over setup, with the percentage increasing/decreasing with increasing/decreasing tidal elevation over the reef flat. In particular, IG variability is an important component of reef water level extremes that adds to previous studies that have considered wave setup [Hoeke *et al.*, 2013] and SS waves [Storlazzi *et al.*, 2011].

The component approach is needed for making estimates at sites where the specific empirical parameters developed for the RMI sites may not apply. For general applications, there are a number of simplifications to (3) and (6) that reduce the reliance on site-specific parameterizations. For setup, the analytic expression (3) may be directly applied with estimates of γ_s . The effect of ignoring the tidal dependence of γ_s generally leads to a 10–20% overestimate of setup at high tides [Becker *et al.*, 2014a]. The estimation of H_{ig} requires specification of the friction parameter, D , which, for smooth reef flats such as found at Roi and CMI, values of 0.005–0.007 are likely to be sufficient. The spectral character of the breaking wave envelope also is required to estimate H_{ig} . In future work, we will consider possible parameterizations of the wave height envelope spectrum based on deep water wave conditions. As mentioned, a general estimate of H_{ss} requires knowledge of the ratio of wave height to water depth at the outer reef flat [Becker *et al.*, 2014a].

Thus, for general extreme water level estimates, information is required of the breaking wave height and depth, the spectral character of the breaking wave envelope, the depth, width, and frictional roughness of the reef flat. Given the general lack of direct wave observations available in the Pacific Island region, wave models such as Durrant *et al.* [2013] are a valuable resource that can be extended using the parameterizations described here. Further work is needed to extend the extreme water level estimates, which pertain to conditions just prior to reaching the shoreline, to runup levels.

References

- Becker, J. M., M. A. Merrifield, and M. Ford (2014a), Water level effects on breaking wave setup for Pacific Island fringing reefs, *J. Geophys. Res. Oceans*, 119, 914–932, doi:10.1002/2013JC009373.
- Becker, J. M., M. A. Merrifield, M. Ford, and H. Yoon (2014b), Long waves in the Marshall Islands: Observations and theory, Abstract 15032, paper presented at 2014 Ocean Sciences Meeting, ASLO/AGU/TOS, Honolulu, HI, 23–28 Feb.
- Durrant, T., M. Hemer, C. Trenham, and D. Greenslade (2013), *CAWCR Wave Hindcast 1979-2010*. v5. CSIRO. Data Collection, doi:10.4225/08/523168703DCC5.
- Ferrario, F., M. W. Beck, C. D. Storlazzi, F. Micheli, C. C. Shepard, and L. Airoidi (2014), The effectiveness of coral reefs for coastal hazard risk reduction and adaptation, *Nat. Commun.*, 5, 3794, doi:10.1038/ncomms4794.
- Ford, M. R., J. M. Becker, and M. A. Merrifield (2013), Reef flat wave processes and excavation pits: Observations and implications for Majuro Atoll, Marshall Islands, *J. Coastal Res.*, 29(3), 545–554.
- Ginoza, L. (1979), Majuro pounded by big surf, *Pac. Daily News*, 10(301), 1.
- Gourlay, M. R. (1996a), Wave set-up on coral reefs. 1. Set-up and wave-generated flow on an idealised two dimensional reef, *Coastal Eng.*, 27, 161–193.
- Hoeke, R. K., K. L. McInnes, J. C. Kruger, R. J. McNaught, J. R. Hunter, and S. G. Smithers (2013), Widespread inundation of Pacific islands triggered by distant-source wind-waves, *Global Planet. Change*, 108, 128–138.

Acknowledgments

This work was supported through a grant from the National Science Foundation (OCE-0927407), with additional funding for Y. Yao provided by the National Natural Science Foundation of China (grant 51309035). Chris Kontoes, Carly Quisenberry, and Derek Young conducted the field experiments, with additional field support provided by Lauren Molina, Chris Colgrove, Melanie Hutchinson, and Bryan Rahter. We are grateful for on-site support provided by U.S. Army Kwajalein Atoll (USAKA) personnel and Don Hess at the College of the Marshall Islands. Nancy Hulbirt provided graphics support. The Kwajalein tide gauge data set, operated by the NOAA Center for Operational Products and Services (CO-OPS), was obtained from the University of Hawaii Sea Level Center. The Wave-Watch III hindcast was provided by CSIRO/BOM (<https://data.csiro.au/dap/landingpage?pid=csiro%3A6616>). Data used in this study are available upon request (markm@soest.hawaii.edu). We thank Curt Storlazzi, Peter Swarzenski, and Joshua Logan of the U.S. Geological Society, Santa Cruz, CA, for sharing their preliminary survey data from Roi-Namur.

Lisa Beal thanks two anonymous reviewers for their assistance in evaluating this paper.

- Lugo-Fernandez, A., H. H. Roberts, and W. J. Wiseman (1998), Tide effects on wave attenuation and wave set-up on a Caribbean coral reef, *Estuarine Coastal Shelf Sci.*, *47*, 385–393.
- Merrifield, M. A., P. R. Thompson, and M. Lander (2012), Multidecadal sea level anomalies and trends in the western tropical Pacific, *Geophys. Res. Lett.*, *39*, L13602, doi:10.1029/2012GL052032.
- Monismith, S. G., L. M. M. Herdman, S. Ahmerkamp, and J. L. Hench (2013), Wave transformation and wave-driven flow across a steep coral reef, *J. Phys. Oceanogr.*, *43*, 1356–1379.
- Munk, W. H., and M. C. Sargent (1948), Adjustment of Bikini Atoll to ocean waves, *Eos Trans. AGU*, *29*(6), 855–860.
- Nakaza, E., and M. Hino (1991), Bore-like surf beat in a reef zone caused by wave groups of incident short period waves, *Fluid Dyn. Res.*, *7*(2), 89–100, doi:10.1016/0169-5983(91)90062-N.
- Péquignet, A.-C., J. M. Becker, M. A. Merrifield, and J. Aucan (2009), Forcing of resonant modes on a fringing reef during tropical storm Man-Yi, *Geophys. Res. Lett.*, *36*, L03607, doi:10.1029/2008GL036259.
- Péquignet, A.-C., J. M. Becker, M. A. Merrifield, and S. J. Boc (2011), The dissipation of wind wave energy across a fringing reef at Ipan, Guam, *Coral Reefs*, *30*, 70–82.
- Péquignet, A.-C., J. M. Becker, and M. A. Merrifield (2014), Energy transfer between wind waves and low-frequency oscillations on a fringing reef, Ipan Guam, *J. Geophys. Res. Oceans*, *119*, doi:10.1002/2014JC010179, in press.
- Pomeroy, A., R. Lowe, G. Symonds, A. Van Dongeren, and C. Moore (2012), The dynamics of infragravity wave transformation over a fringing reef, *J. Geophys. Res.*, *117*, C11022, doi:10.1029/2012JC008310.
- Stockdon, H. F., R. A. Holman, P. A. Howd, and A. H. Sallenburg Jr. (2006), Empirical parameterization of setup, swash, and runup, *Coastal Eng.*, *53*, 573–588.
- Storlazzi, C. D., E. Elias, M. E. Field, and M. K. Presto (2011), Numerical modeling of the impact of sea-level rise on fringing coral reef hydrodynamics and sediment transport, *Coral Reefs*, *30*, 83–96.
- Tait, R. J. (1972), Wave set-up on coral reefs, *J. Geophys. Res.*, *77*(12), 2207–2211.
- Torres-Freyermuth, A., I. Mariño-Tapia, C. Coronado, P. Salles, G. Medellín, A. Pedrozo-Acuña, R. Silva, J. Candela, and R. Igelesias-Preto (2012), Wave-induced extreme water levels in the Puerto Morelos fringing reef lagoon, *Nat. Hazards Earth Syst. Sci.*, *12*, 3765–3773.
- Vetter, O., J. M. Becker, M. A. Merrifield, A.-C. Péquignet, J. Aucan, S. Boc, and C. Pollard (2010), Wave set-up over a Pacific Island fringing reef, *J. Geophys. Res.*, *115*, C12066, doi:10.1029/2010JC006455.